Studying Cerebral Blood Flow in Mouse Cortex with Optical Microangiography

Adiya Rakymzhan

A thesis

submitted in partial fulfillment of the

requirements for the degree of

Master of Science

University of Washington

2020

Committee:

Ruikang K. Wang

Azadeh Yazdan-Shahmorad

Program Authorized to Offer Degree:

Bioengineering

University of Washington

Abstract

Studying Cerebral Blood Flow in Mouse Cortex with Optical Microangiography

Adiya Rakymzhan

Chair of the Supervisory Committee:
Professor Ruikang K. Wang
Bioengineering Department

Optical coherence tomography (OCT) is a non-contact three-dimensional (3D) imaging modality which enables fast *in vivo* volumetric visualization of internal structures of biological tissues with high resolution. In this thesis, first, the application of OCT advanced extension - optical microangiography (OMAG) - was used to reveal the temporal profile of hemodynamic response to neural activation and the variation of depth-resolved blood flow changes in mouse cerebral cortex. The results showed that the largest hemodynamic response occurred in cortical layer IV. Second, OMAG and Doppler OMAG (DOMAG) techniques were applied to quantitatively evaluate the anesthesia effect on cerebral vessel morphology and blood flow in mouse model. According to the results, isoflurane and ketamine-xylazine caused vasodilation both in large and capillary vessels, which led to increased CBF. Overall, this thesis demonstrated that OMAG is an effective tool for studying depth-resolved microvasculature and blood flow in animal cortex.

TABLE OF CONTENTS

Chapter 1. INTRODUCTION

1.1 Significance and research motivation

A regional increase in cerebral blood flow (CBF) during local neural activation is associated with neurovascular coupling (NVC), which is also referred to as functional hyperaemia.[1] NVC is a vital process, which regulates oxygen delivery through blood stream to supply the activated neurons for normal brain functioning.[1] Therefore, studying the mechanisms of CBF regulation at NVC is crucial for the improved understanding of brain activity under normal and neurodegenerative conditions.

1.2 Current methods and scientific gap

Number of imaging modalities have been applied to study CBF. Traditional imaging methods such as functional magnetic resonance imaging (fMRI) [2] and positron emission tomography (PET) [3] are limited in spatial and temporal resolution to detect hemodynamic responses. Optical imaging techniques offer a broad range of contrast mechanisms and can be readily applied to animal studies to measure CBF parameters. However, assessing all these parameters with a single technique is still challenging. For instance, laser Doppler imaging (LDI) is great at evaluating blood flow, but has to compromise between spatial and temporal resolution. [4] Photoacoustic microscopy (PAM) can provide information about vascular morphology and flow, but requires physical contact with the object. [5] Intrinsic optical signal imaging (IOSI) [6] and laser speckle imaging (LSI) [7] are excellent full-field imaging tools for measuring CBF and blood oxygenation. Although the given technologies are widely used, their detection is two-dimensional (2D) with no

access to deep-layer structures. Three-dimensional (3D) imaging methods, such as two-photon laser scanning microscopy (TPM) [8-10] and confocal laser scanning microscopy (CLSM) [11] have been proven effective in studying neurovascular dynamics. However, they both cannot have sufficient field of view (FOV) without compromising spatial resolution and require contrast agent injection. [12] Thus, there is a pressing need for *in-vivo* non-contact 3D depth-resolved technology capable of imaging CBF with a high spatiotemporal resolution.

1.3 The advantages of optical coherence tomography (OCT)

In contrast to other micro-scale resolution imaging modalities, optical coherence tomography (OCT) enables high-resolution three-dimensional (3D) visualization and quantification of internal structures in biological tissues up to 2 mm beneath the tissue surface. [13] In OCT angiography (OCTA) extension – optical microangiography (OMAG), the dynamic complex OCT signal from moving red blood cells (RBCs) is analyzed to acquire blood vessel and flow information down to capillary level. [14] Another angiography method named Doppler OMAG (DOMAG) is based on phase-resolved technique and allows to measure the axial velocity of RBCs in penetrating vessels. [15] These advantages make OCT a useful tool for studying cerebral vasculature and hemodynamics in animal models.

1.4 The scope of the thesis

The objective of this thesis is to demonstrate the application of OCTA methods in studying cerebral blood flow in mouse model. The first part of this thesis will be focused on examining the temporal profile of hemodynamic change in response to neural activation and the variation of depth-resolved

blood flow changes in mouse cerebral cortex using OMAG method. The second part of the thesis will apply OMAG and DOMAG techniques to quantitively analyze the difference in cerebral blood vessel morphology and flow between awake and anesthetized regimes in mouse model.

Chapter 2. METHODS

In this chapter, I will briefly introduce the optical imaging methods I have applied in this thesis study.

2.1 ISOI

ISOI is a 2D *in vivo* optical imaging technique that is widely used for functional brain mapping in animal models. It is label-free and has a relatively good spatial and temporal resolution. The working principle of ISOI is based on cortical reflectance change due to hemodynamic response. One of the main sources of intrinsic signals in brain is the change of absorption of intrinsic chromophores such as hemoglobin. Deoxygenated (Hb) and oxygenated hemoglobin (HbO) are equally absorbed at spectral range of 530-565 nm, which makes their detection independent of oxygen variations and sensitive to hemoglobin (HbT) content in the total blood volume. Once cortical region is functionally activated, it induces the hemodynamic response such as local increase of cerebral blood volume (CBV). As a result, the amount of HbT also locally grows which leads to higher light absorption. The difference between an unstimulated baseline and local hemodynamic response provides a reflectance contrast. [16] The IOSI setup I used in this study is demonstrated in Fig. 1. The *in vivo* mouse cortex is illuminated with a 532-nm laser source and the reflected light is detected by an area-scan camera.

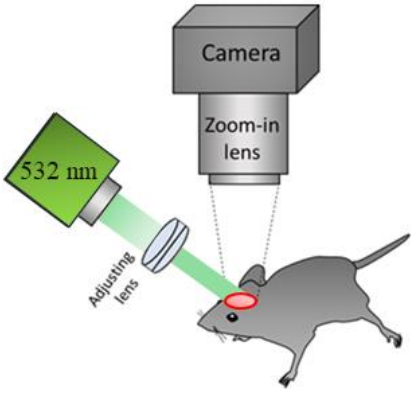

Figure 1. ISOI setup.

2.2 OCT

OCT is an optical imaging modality that is able to generate volumetric images of biological tissues with microscopic resolution in real time. [13] The working principle of OCT (Fig. 2) is based on a low-coherence interferometer. Thus, the light from a light source is directed onto a beam splitter and is split into a reference and a measurement beam. The measurement beam is backscattered from the sample with different time delays according to its internal microstructure. The reference beam is reflected from a reference mirror at an alternating distance which produces an alternating time delay. The backscattered light from the sample is combined and interfered with the reflected light from the reference mirror, which can occur only when the two path lengths match to within the coherence length of the light. The echo time delay and intensity of backscattered light from layers of the sample can be measured by detecting and demodulating the interference signal while scanning the reference path length. This type of OCT system is known as a time-domain OCT. [17]

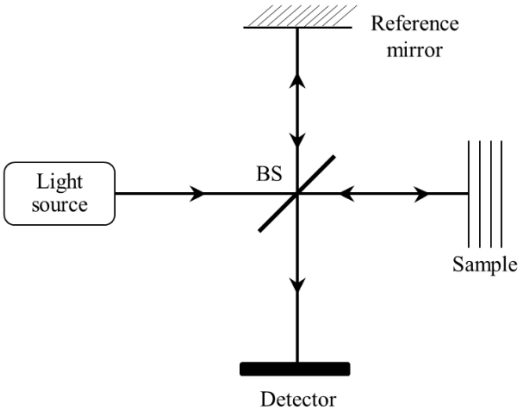

Figure 2. Schematic illustration of OCT working principle. BS: beam splitter.

Since the invention of OCT, the technology has been improving both in imaging method and imaging analysis. Thus, frequency-domain OCT has been developed, which significantly improved data acquisition speed and axial resolution of the system. Frequency-domain OCT does not physically scan a reference mirror, which eliminates the need to mechanically move the reference arm. Instead, it detects the backscattered signal in frequency domain using Fourier transform. Therefore, this version of OCT was named Fourier-domain OCT (FD-OCT). [18]

The spectral-domain OCT (SD-OCT) is a type of FD-OCT, which includes diffraction grating and linear detector such as shown in Fig. 3. In this study, I used an in-house built SD-OCT system to image mouse cerebral cortex *in vivo*. The system was equipped with a superluminescent diode (SLD) with a center wavelength of 1310 nm and a spectral bandwidth of 110 nm which provided ~7.5-μm axial resolution in air (~ 5.1 μm in mouse brain tissue). In the sample arm, divided by a 2 × 2 optical coupler, one part of SLD light passed through the optical system composed of a collimator, X-Y galvanometer and an 10X objective lens with 10-μm lateral resolution. The rest of the light was directed into the reference arm through a collimator and lens. The light reflected from the sample interfered with the reference light. Next, to detect the interference signal, the output light was transmitted to a spectrometer with a spectral resolution of 0.141 nm, which

provided 2.22 mm imaging depth into the sample. The spectrometer was equipped with an InGaAs line scan camera with 92 kHz A-line rate to capture the interference signal.

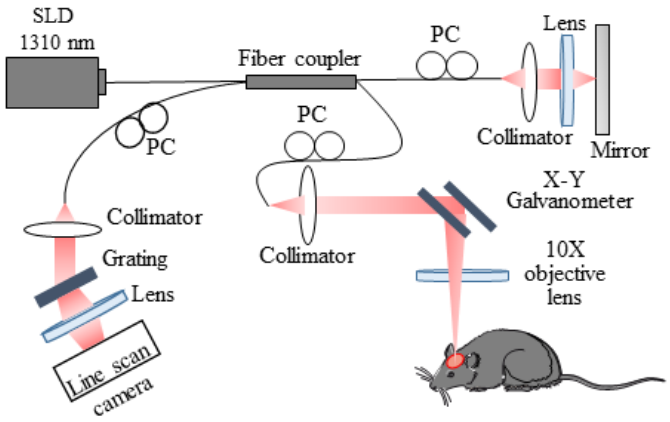

Figure 3. Schematic diagram of in-house built SD-OCT system. SLD: superluminescent diode, PC: polarization controller.

Depth information in OCT scanning is represented by A-line (A-scan) and referred to as z axis (Fig. 4). Multiple A-scans in the transverse direction (x axis) form a B-scan (OCT cross-sectional image). B-scans are measured at several transverse positions (y axis) to produce a 3D data set. *Enface* image is the x-y projection of 3D dataset over a given depth or at a particular depth layer.

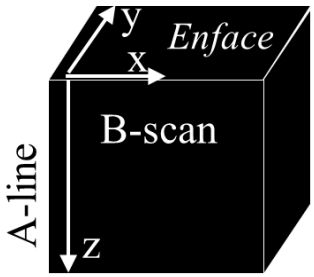

Figure 4. Schematic diagram of OCT data structure.

2.2.1 OMAG

OCTA is an umbrella term for scanning protocols and post-processing algorithms focused on enhancing the motion contrast of RBCs in OCT images to highlight functioning blood vessels. [19] All OCTA methods start from complex OCT signal *S* which can be expressed as:

$$S(x,z,t) = I(x,z,t)e^{-i\Phi(x,z,t)},$$

where I is the amplitude component and Φ is the phase component. OCTA algorithms are categorized into intensity-, phase-, and complex-signal-based types. [19] OMAG is a complex-signal-based OCTA method, where signals from moving particles are separated from the static tissue signals. [14] The OCT signal at each imaging voxel is considered as a superposition of three independent components: clutter (static and slowly moving tissue structures), blood flow signal (moving RBCs), and noise (system and shot noise). The given signal is presented in the form of correlation matrix, where the clutter components are decomposed into eigenvectors and eigenvalues. The first two highest power eigenvalues corresponding to tissue bulk motion are excluded from the covariance matrix among the repeated B-scans to produce blood flow OMAG images. [20]

2.2.2 DOMAG

DOMAG is the combination of Doppler OCT and OMAG technologies. Doppler OCT is a phase-resolved technique used to extract blood flow velocity information from functional vessels. [21] The main advantage of OMAG algorithm is that static tissue signal is separated from blood flow signal making it almost free of artifact noise. Thus, the axial velocity of RBCs can be measured by calculating the phase difference between adjacent A-lines from OMAG flow signal [21]:

$$v_{axial} = \frac{\lambda\varphi}{4\pi nT},$$

where λ is the light source center wavelength, φ is the phase difference, n is the tissue refractive index, and T is the time interval between adjacent A-lines. To detect slow velocities in capillaries, longer T value is required. Therefore, the method was improved by providing a variation of T values for detecting multiple range velocities. [15] Thus, DOMAG allows to measure the axial RBC velocity both in capillaries and large vessels.

Since vessels perpendicular to the cortical surface are the most sensitive for detection of axial RBC velocity, the DOMAG is applied to cerebral penetrating vessels. [15] The blood flow rate can be obtained from penetrating vessels by integrating the velocity over the flow area:

$$Flow = \iint_{xy\ area} v_{axial}(x, y)\, dxdy$$

Based on previous study validation [22], the flow calculation does not require the calculation of vessel angle. Thus, using the cross-sectional area of the penetrating flow and flow rate within this area, DOMAG also allows to quantify CBF.

Chapter 3. OMAG REVEALS TEMPORAL AND DEPTH-RESOLVED HEMODYNAMIC CHANGE IN MOUSE BARREL CORTEX DURING WHISKER STIMULATION

3.1 Background and motivation

The variation of neuronal density among six cortical layers results in different metabolic demands, and consequently, different blood flow adjustments. [23] Accordingly, several studies have demonstrated the variation of hemodynamic response to neural activation over cortical depth. Particularly, the studies with functional magnetic resonance imaging have shown the increase of blood oxygenation level-dependent (BOLD) signal in the center of cortex [24] and the fastest response in deep layers. [25] A more specific investigation with two-photon microscopy on capillaries revealed the most pronounced changes in red blood cells (RBCs) velocity and flux beyond the depths of 200 μm. [26] In other research study using dynamic contrast optical coherence tomography, the shortest mean transit time and capillary transit time heterogeneity were observed in the layers 4 and 5. [27] Despite all the experimental findings and explorations, there is still a lack of depth and temporal information on hemodynamic variation across the cortex. This challenge invokes in-vivo 3D depth-resolved functional imaging of CBF with a high spatiotemporal resolution such as OMAG.

In previous studies, OMAG was applied to measuring the capillary blood flow in mouse cortex. [28] OMAG also allowed for measuring the velocity and transit time of capillary red blood

cells in mouse somatosensory cortex. [29] However, these studies have examined neither the temporal profile of hemodynamic change in response to neural activation, nor the variation of depth-resolved blood flow changes.

In this study, we employed OMAG and IOSI to image the activated somatosensory cortex of mouse brain. Temporal profiles of both signals are compared, and depth differentiated OMAG blood flow changes during functional activation are observed and discussed to provide additional insight of hemodynamic regulation at the NVC.

3.2 Materials and methods

3.2.1 Animal preparation

Animal surgeries and experimental procedures in this study were approved by the Institutional Animal Care and Use Committee (IACUC) of the University of Washington and conduced in accordance with University of Washington guidelines and ARRIVE guidelines. C57BL/6 mice (Charles River Laboratories, n=6, 3-month-old, 23–25 g) were anaesthetized with a Ketamine/Xylazine cocktail (0.1 ml/ 25 g mouse, IP). Physiological parameters such as adequate anesthesia depth (no hindpaw reflexes) and body temperature (36.8±0.2 ℃) were monitored throughout all experimental procedures. Optical access to the somatosensory cortex was obtained through a cranial window surgery in the left cerebral hemisphere according to protocol described in Ref. 30 [30]. In brief, after the skin and meninges tissues were removed from the skull surface, a window opening was drilled in the skull and the exposed brain was sealed with a 5-mm circular glass coverslip using glue.

3.2.2 IOSI

IOSI was performed to spatially localize the hemodynamic response in mouse cortex. The exposure time of the camera was set to 40 ms and the frame size was 1280 × 1024 pixels representing 5.5 × 5.5 mm of cortical area. In total, 525 frames were acquired within 35 s.

For the analysis (Fig. 5A), a baseline was obtained by temporal averaging of the first 10 frames. The baseline was then subtracted from every frame, and the resulting frames were normalized to the baseline. Two-dimensional reflectance images and time-lapsed reflectance signal profiles at both activated region (R1) and the non-activated regions (R2) were presented. At each region, the change in reflectance signal (-ΔR/R) was averaged across 6 animals.

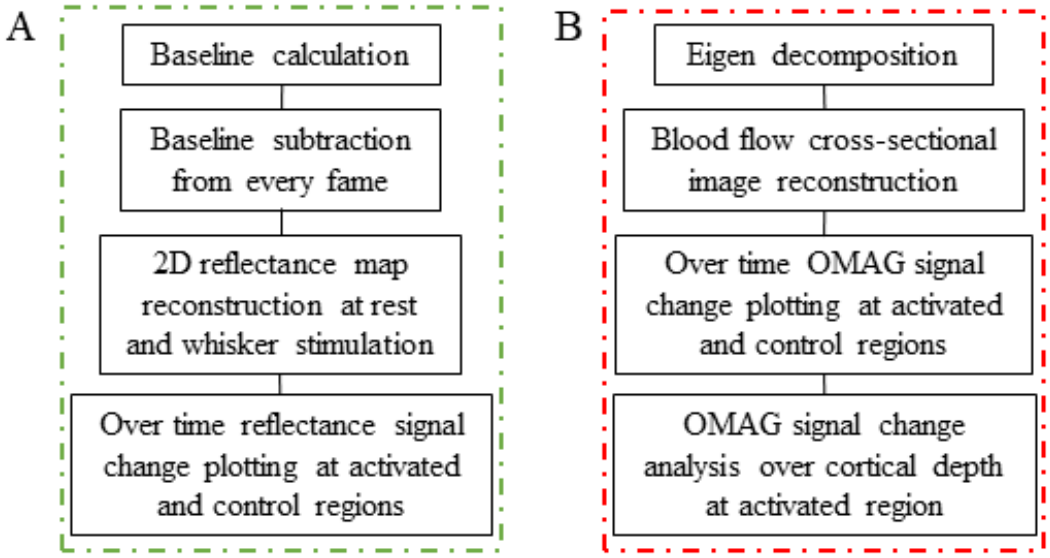

Figure 5. Flowchart of data analysis. A. Algorithm for IOSI data analysis. B. Algorithm for OMAG data analysis.

3.2.3 OMAG

The scanning protocol was the repeated B-scans with a scan rate of 300 fps. Every B-scan was formed by 200 A-lines at a rate of 92 kHz. In total, 10500 frames were acquired within 35 s, covering an approximate cross-sectional region of 1.4 mm (x axis) x 2.22mm (z axis) with a

uniform transverse sampling of 7.5 μm/pixel. Imaging was performed at activated and control regions identified by IOSI during rest and stimulation periods.

Cross-sectional OMAG images and signal change time profiles at both activated region (R1) and the non-activated regions (R2) were then demonstrated. For the time profiles, the same strategy as for IOSI was applied: a temporally averaged baseline over first 10 frames was subtracted from every frame, and the resulting frames were normalized to the baseline. The analysis of OMAG signal changes over cortical depth was also presented. The step-by-step algorithm for OMAG data analysis is presented in Fig. 5B. The OMAG intensity signal was averaged across 6 animals.

3.2.4 Stimulation

Mouse whiskers were mechanically stimulated with a wood stick attached to a stepper motor (Fig. 6). A wood stick was positioned 5-7 mm from the mouse face. The motor operating at a rate of 3Hz was synchronized with both imaging systems. The motor was triggered at the 5th second of data acquisition and continued for 10 s. Each trial was 35 s in total, including 5 s of rest, 10 s of stimulation, and 20 s of post-stimulation rest. There was one trial per each animal.

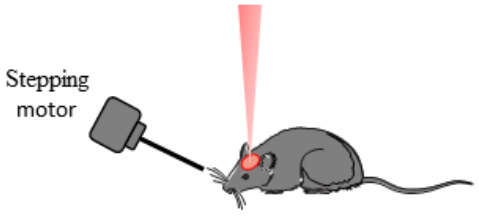

Figure 6. Schematic illustration of whisker stimulation with a stepping motor.

3.2 Results

3.3.1 Reflectance signal change upon functional activation

To locate the barrel cortex area, first, we imaged the cranial window (Fig. 7A) with IOSI before (0-5 s), during (5-15 s) and after (15-35 s) whisker stimulation. Figure 7B represents the reflectance

image at the resting state (2^{nd} s from the onset of imaging) and Fig. 7C shows the reflectance image at the functional activation (12^{th} s). The latter demonstrates the localized increase of signal reflectance during whisker stimulation at the region R1, which corresponds to barrel cortex [31], and no pronounced change of reflectance at the region R2 (which was thus considered as the control in this study). The variation of the reflectance signal over time at the activated (R1) and non-activated (R2) regions averaged over 6 animals are presented in Figure 7D. The dashed line indicates the start (5^{th} s) and the end (15^{th} s) of stimulation period. The reflectance signal curve at the region R1 shows an obvious response peak, starting to rise within 1 s since the onset of stimulation. It peaks at approximately 15^{th} s (about 35% increase from the baseline), then gradually decreases, and finally reaches its plateau at around 21^{st} s. There is a very slight response at non-activated region R2 following the same trend. Here we demonstrated the ability of our IOSI system to accurately detect the spatial and temporal reflectance response to the functional activation. The given method confirmed the stimulus-evoked activation at barrel cortex and provided further guidance for studying hemodynamic response in mouse cortex using OMAG.

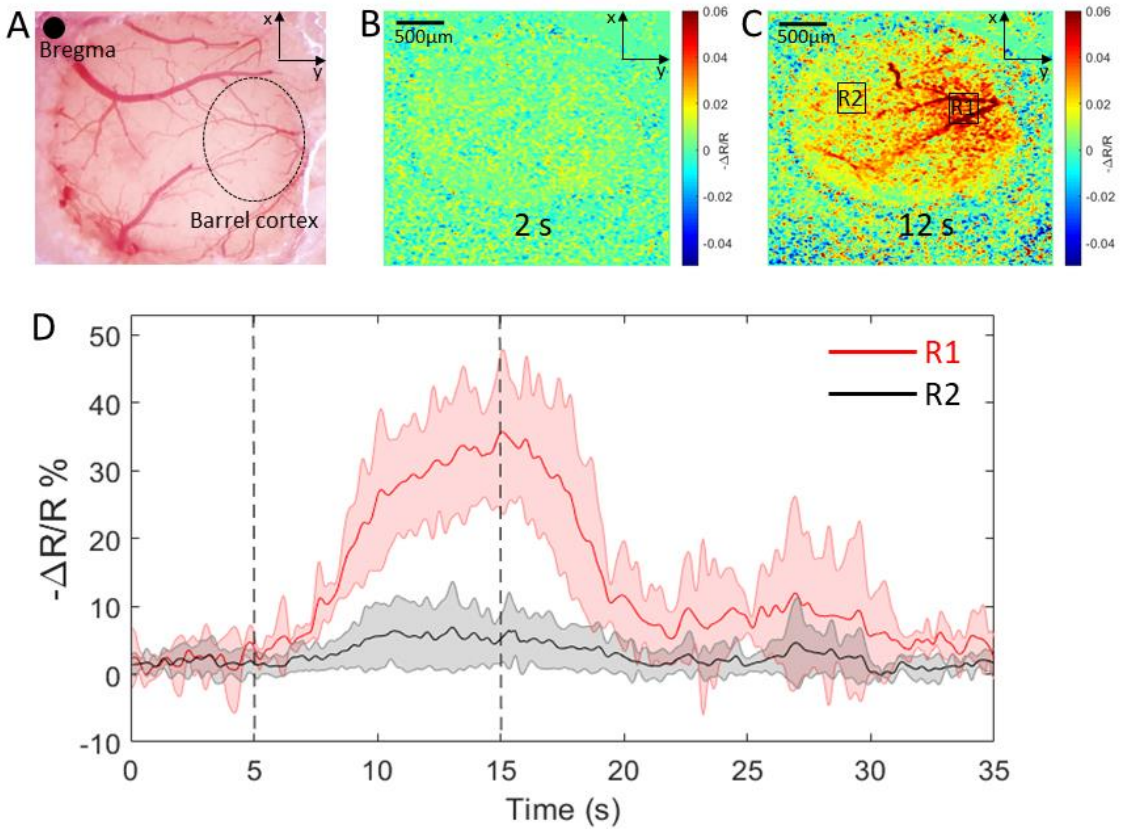

Figure 7. IOSI identifies the activation region in the brain cortex upon whisker stimulation. A. Microscope image of cranial window at somatosensory cortex. B. Reflectance map of cranial window area at resting (2nd s). C. Reflectance map of cranial window area at stimulation (12th s). R1 indicates the activated region and R2 indicates the control region. D. Temporal profile of reflectance signal change in response to whisker stimulation at activated (red curve) and control (black curve) regions averaged across 6 animals. The shaded error bar indicates the signal variation over 6 animals. ΔR is a change in reflectance signal, R is a baseline reflectance signal. Dashed lines indicate the start and the end of stimulation time.

3.3.2 OMAG signal change upon functional activation

Guided by reflectance maps obtained by IOSI above, we imaged mouse cortex with OCT at the location indicated by the dashed line in Fig. 8A. As a result, cross-sectional OCT image of cortex structure is presented in Fig. 8B and cross-sectional OMAG image of cortex blood flow is shown in Fig. 8C. Temporal profiles of OMAG signals averaged over 6 animals were obtained from activated (R1) and control (R2) regions (Fig. 8D). There is a clear reaction of OMAG signal intensity due to functional activation, which lasted from 5th to 15th s. The response started within 1 s once the whisker stimulation began and reached its maximum (increase of approximately 12%)

in about 5 s. The intensity dropped once stimulation ended and eventually ran into plateau at about 20th s. These results showed that OMAG is a useful tool for time course investigation of hemodynamic change in response to neural activation.

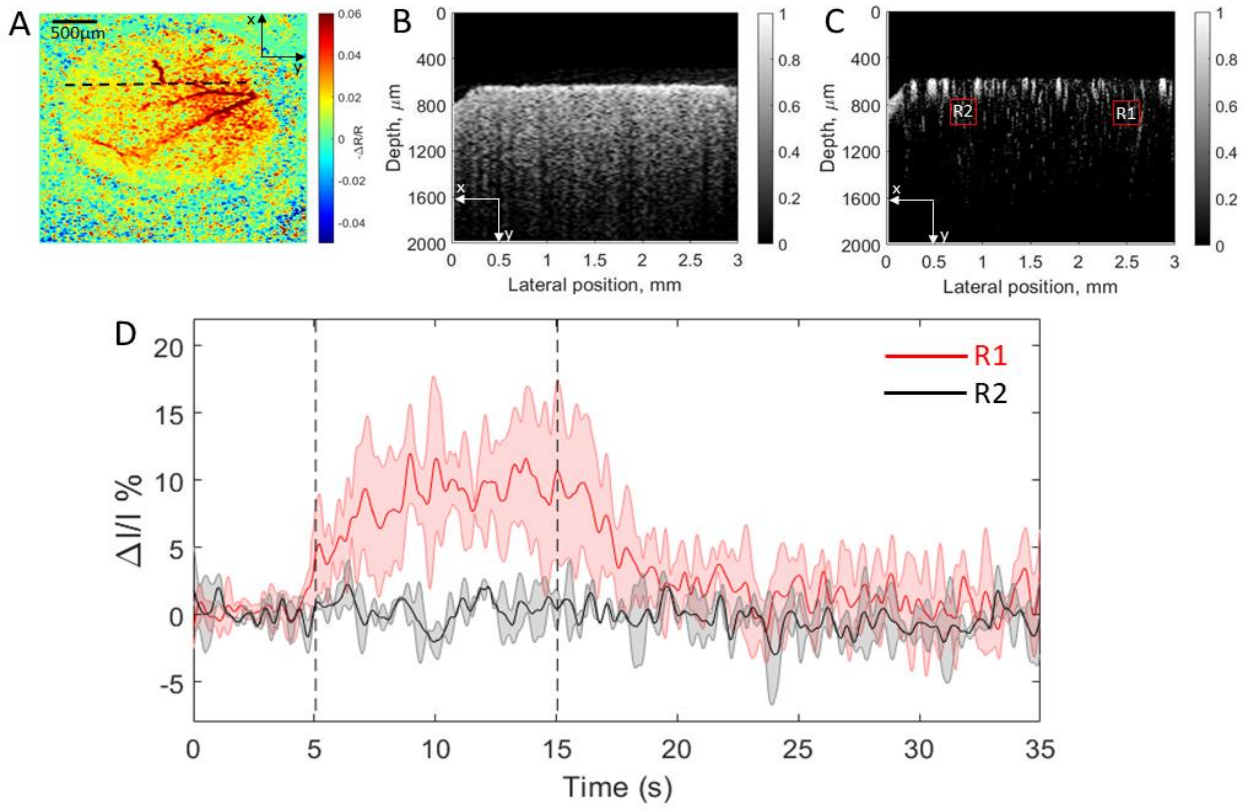

Figure 8. OMAG provides an ability to detect the localized hemodynamic response within the brain cortex upon whisker stimulation. A. Reflectance IOSI map of the cortical tissue at cranial window, where the dashed line indicates the cross-section position for OCT imaging. B. Cross-section of OCT structural image. C. Cross-section of OMAG blood flow image. R1 indicates the activated region and R2 indicates the control region. D. Temporal profile of OMAG signal change in response to whisker stimulation at activated (red curve) and control (black curve) regions averaged over 6 animals. The shaded error bar indicates the signal variation over 6 animals. ΔI is the change in OMAG signal, and I is the baseline OMAG signal. Dashed lines indicate the start and the end of stimulation time.

3.3.3 OMAG signal variation over depth

Next, we examined the change of the OMAG signal over cortical depth at activated region. Figure 9A illustrates the selected cross-sectional region and Fig. 9B shows the approximate location of selected layers I, II/III, IV and V, corresponding to 50-100 μm, 185-235 μm, 360-410 μm, and 500-550 μm, respectively. [32] First, OMAG signal was spatially averaged over every layer, and

temporally averaged over the time periods before and during stimulation. The average of the signal intensity before stimulation (I_{rest}) was subtracted from the average of the signal during stimulation (I_{stim}), and normalized by the average of signal intensity at rest (I_{rest}). This gave the percent value of OMAG signal change in response to neural stimulation. The obtained value was averaged over 6 mice and plotted in bar graph in Fig. 9C. Interestingly, the largest difference in intensity between resting and stimulation states was revealed in layer IV. One-way ANOVA followed by Tukey's honestly significant difference test for multiple comparisons was performed to assess how significantly the OMAG signal difference varied across the layers. The statistical results showed a significant difference between layers I and IV (p-value=0.02), layers II/III and IV (p-value=0.03). This experimental finding demonstrates that OMAG could be a useful tool to detect the layer-specific hemodynamic changes.

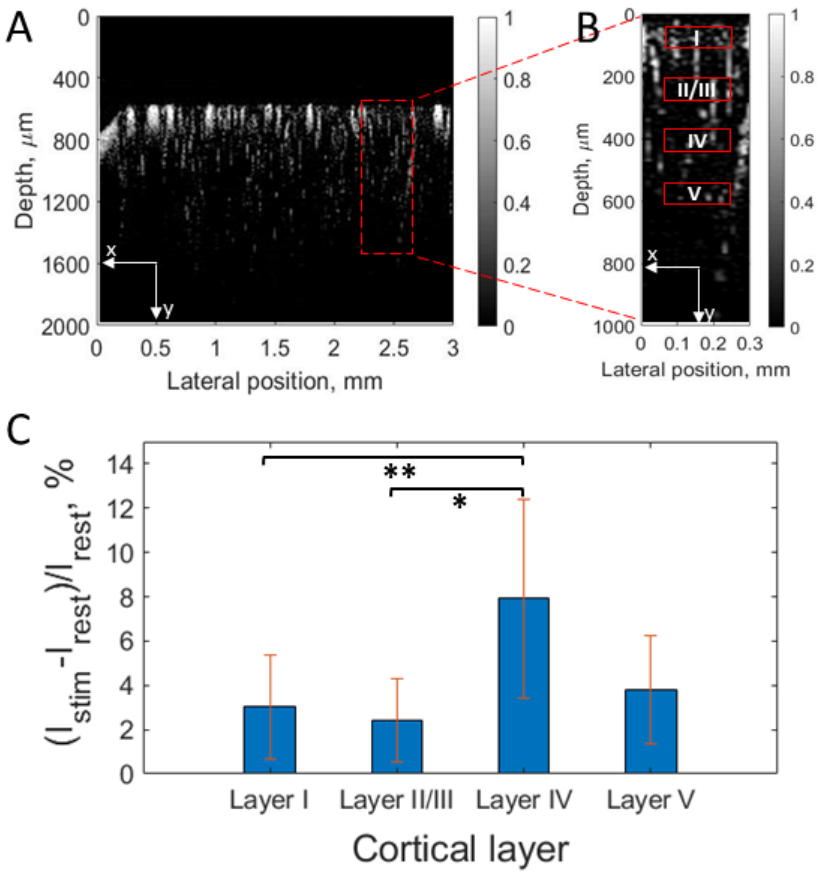

Figure 9. OMAG provides an ability to detect the variation of hemodynamic response over cortical depth upon whisker stimulation. A. OMAG cross-sectional blood flow image with activated region indicated (red rectangle). B. OMAG cross-sectional blood flow image of activated region indicated in A with layers' location indicated. C. Difference in OMAG signal intensity between rest and functional activation states over cortical depth averaged over 6 animals. Error bars represent the standard deviation. *p-value<0.02, **p-value<0.03.

3.4 Discussion

Cerebral blood flow (CBF) regulation at neurovascular coupling (NVC) plays an important role in normal brain functioning to support oxygen delivery to activating neurons. Hemodynamics-based non-invasive imaging techniques such as intrinsic optical signal imaging (IOSI) and optical microangiography (OMAG) have proven effective in providing CBF information during neural activity. However, the combined application of these two methods to study brain functional

activation has yet to be explored. In this study, we used OMAG guided by IOSI reflectance signal map to image the somatosensory cortex of mouse brain.

OMAG is based on complex OCT signals which include both intensity and phase information. The OMAG signal is considered to be a product of moving particle velocity and its concentration. In other words, it is the total number of RBCs passing through the imaging voxel area per unit time. Therefore, the OMAG signal magnitude represents the blood flow flux and depends on blood flow velocity and hematocrit values.[33] Choi et al. [33] demonstrated that at 3.6 ms interval between adjacent B-scans, OMAG signal does not have strong relationship to RBC velocity, nor it is dependent on the size of vessels (vessel diameter). The reason is that for the time interval beyond 3 ms, the OMAG magnitudes are fully saturated for the flow velocities faster than 0.1 mm/s. However, it was found that particle concentration has a significant impact on OMAG intensity. Given that the time interval in our study is ~3.3 ms and typical velocity for blood flow is faster than at least 0.3 mm/s, it is reasonable to assume that the velocity would saturate the OMAG signal, and the increase of OMAG signal from the mouse CBF during neural stimulation is a result of the increase of RBCs, i.e. hematocrit. Nevertheless, it has to be noted that the specified phantom experiment was done with Intralipid solution, which has totally different optical properties from the blood. In other study with OCT angiography (OCTA), microfluidic channels filled with human blood were imaged. [34] It was shown that in large channels, hematocrit has little effect on OCTA intensity, yet in smaller channels of a capillary size, the flow signal substantially depends on hematocrit value. Thus, in the middle layers of mouse cortex where there is a dense capillary network [35], RBC concentration change might considerably affect the OMAG signal in in vivo experiments. In fact, the *in vivo* study with laminar optical tomography (LOT) suggests that a net increase in the linear density of RBCs in the capillaries accompanies the flow

response to functional stimulus, which was explained by the increase of RBC stacking due to capillary dilation that occurs during stimulus response. [36] The expansion of capillary diameter allows a higher plasma volume flow, but is not sufficient to allow more than one RBC to pass at the same time, which results in an increased RBC stacking linear density. Previous study with OCTA [37] also showed that RBC content increases over functional activation and most prominent increase occurs in the middle cortical layer. Thus, within a particular range of a time interval between consecutive B-scans, the OMAG signal might be effectively used as an indicator of blood flow flux change associated with the hemodynamic response.

In this study, we used IOSI and OMAG to image the barrel cortex of mouse brain. Our IOSI system accurately detected the spatial and temporal reflectance response to whisker stimulation, confirming the stimulus-evoked activation at barrel cortex. Guided by IOSI reflectance maps, OMAG was able to provide temporal profile of intensity signal change caused by functional activation at activated and non-activated regions of mouse cortex. Our results demonstrated ~35 % increase of IOSI signal in response to neural stimulation, while the OMAG signal rose by only ~12 % (Fig. 2D and Fig. 3D). Such a difference in response signal magnitude may be explained by the difference in the signal sources. IOSI detects the absorbed light which might include the absorption by HbT and scattering inside the tissue. Whereas, OMAG is sensitive to backscattered signal from moving RBCs.

From the time courses of IOSI reflectance signal and OMAG signal change, we observed that both responses started approximately at the same time. However, OMAG signal reached its peak in about 5 s once functional activation began and stayed at the top until activation ended, while the IOSI reflectance signal grew more gradually and hit its maximum at 10^{th} s after stimulation starts. This phenomenon might be explained by the fact that the region for ISOI signal measurement

contained big arteries (Fig. 7C), while OCT measurement was taken primarily from the capillary network area (Fig. 8C). The previous study with LOT [36] suggests that the rate of arterial HbT increase is slower than that of the capillary bed response. Although OMAG is not sensitive to HbT absorption, it is sensitive to the concentration of RBCs, which are the carriers of HbT molecules.

OMAG also revealed the laminar variation of hemodynamic response to neural activity over cortical depth. The results of our analysis showed that the largest response of OMAG signal to stimulation occurred in the layer IV of cortex. Our results agree with the previous studies on depth-dependent hemodynamic regulation where the most significant hemodynamic response was observed in the fourth cortical layer. [37] The variability of hemodynamic response over cortical layers might be explained by the ability and necessity of brain to adapt the CBF locally to satisfy local metabolic demands [23], since every cortical layer has a different function (neural response, energy use, connectivity) and morphology [38].

Overall, we believe that our findings provided an important opportunity to advance the understanding of hemodynamic events associated with the NVC. The OMAG technique we propose may prove to be a useful tool to investigate the depth-resolved variation of CBF in a fast way without any contrast agents required.

3.5 Conclusion

To conclude, the role of imaging techniques used to quantify the hemodynamics during functional activation is essential for studying the CBF adjustment at the NVC. In this study, we have demonstrated the development and application of a dual-modality imaging system composed of IOSI and OMAG. The results of our feasibility study showed that in addition to IOSI surface blood flow information, OMAG was able to provide complementary blood flow information at the depth

of mouse somatosensory cortex. We believe that OMAG has a potential to enable the future investigation of depth resolved CBF and to provide the insights of hemodynamic events associated with the NVC.

Chapter 4. OMAG REVEALS HEMODYNAMIC DIFFERENCE AT THREE DIFFERENT REGIMES: AWAKE, ISOFLURANE, KETAMINE/XYLAZINE

4.1 Background and motivation

The use of *in vivo* animal models for imaging CBF is crucial for understanding the mechanisms of CBF regulation and brain function. Most of the *in vivo* optical imaging studies have been done in anesthetized animals due to necessity to minimize the motion during image acquisition and eliminate the stress for animals. However, different anesthetics have been proven to disrupt the dynamics of cerebral vasculature. [39] As a consequence, anesthesia greatly impacts the baseline CBF, which can potentially cause discrepancies in interpreting the experimental results of hemodynamic response and cerebrovascular disease studies. [40] Therefore, it is important to study the effect of anesthesia on baseline cerebral hemodynamics in animal models.

Previous studies report the difference in hemodynamic signal in response to functional stimulation between anesthetized and awake conditions in mouse [41-43], rats [44] and marmosets [45]. However, very few of them provide an evaluation of baseline CBF. The vasodilatory effect of isoflurane anesthesia on cerebral microvessels as well as the reduction in blood flow speed were quantified in marmoset cortex, yet only at the individual-vessel level. [45] Although the baseline hemodynamics and oxygen metabolism altered under isoflurane were assessed with quantitative photoacoustic microscopy in mouse brain, the study was focused on big vessels and excluded the

capillary response assessment. [46] Lack of quantitative information on basal CBF parameter according to experimental regime invokes more detailed analysis at both macro- and microvascular levels.

In this study, we applied a combination of OMAG and DOMAG methods to compare the vascular and flow parameters in mouse cortex between anesthetized and awake regimes. The effect of isoflurane and ketamine-xylazine on cerebral vessel and flow dynamics was examined by measuring the changes in artery and vein diameter, capillary density and flux, RBC axial velocity and total blood flow.

4.2 Materials and methods

4.2.1 Animal preparation

Animal surgeries and experimental procedures in this study were approved by the Institutional Animal Care and Use Committee (IACUC) of the University of Washington and conduced in accordance with University of Washington guidelines and ARRIVE guidelines. Six C57BL/6 mice (Charles River Laboratories, 3-month-old, 23–25 g) were used in this study. One day prior the surgery, each mouse was weighed and housed in a separate cage. Next, every animal underwent a surgical procedure to implant a cranial window for optical access [30] followed by a 7-day recovery. To acclimate mice to experimental environment and imaging setup, they were trained for at least 4 days in the laboratory.

4.2.2 Awake imaging

For experiments in awake mice, we placed the animal in a Mobile HomeCage (Neurotar Oy Ltd) which included a head-restraining apparatus and an air-floating cage. Although the mouse was

head-restrained, it was able to freely walk/run or remain stationary during imaging. Each imaging session lasted for about 20 minutes.

4.2.3 Anesthetized imaging

To image the same six mice under anesthesia, we replaced Mobile HomeCage with a stereotaxic frame with a heating pad. Two types of anesthetics have been used: 1) isoflurane (1.5-2%, Baxter) in combination with a mixture of 0.2 L/min pure oxygen and 0.8 L/min air through a nose cone; 2) ketamine HCl (Fort Dodge Animal Health)-xylazine (Lloyd Lab Inc) cocktail (0.1 ml/ 25 g mouse), intraperitoneal. Physiological parameters such as adequate anesthesia depth (no hindpaw reflexes) and body temperature (36.8±0.2 °C) were monitored throughout all experimental procedures. All six mice were imaged under both isoflurane and ketamine-xylazine anesthesia.

4.2.4 Imaging timeline

After the completion of animal training, awake imaging was performed, followed by imaging at isoflurane state immediately. Imaging under ketamine-xylazine was performed 24 hours later, so that animal could fully recover from isoflurane, and anesthetic effects would not interfere.

4.2.5 OMAG

To obtain 3D OMAG images, the repeated B-scan protocol described in Ref. 13 [13] was applied to image the volumetric vasculature. In this protocol, every B-frame was formed by 400 A-lines (z axis) at A-scan rate of 72 kHz. B-frame was repeated 8 times at each transverse location (x axis), and a total of 400 locations was recorded in the C-scan direction (y axis) with a scan rate of 180 frames/sec (fps). Thus, the final 3D volumetric data set consisted of 3200 B-frames taking ~15 seconds to acquire and forming a cube of approximately 2.5 mm (x axis) x 2.5 mm (y axis) x

2.22mm (z axis). Four quadrants were acquired, and the final image (4mm x 4 mm) was automatically stitched from 4 angiograms with ~1-mm overlap.

4.2.6 DOMAG

To obtain 3D DOMAG images, the repeated A-scan protocol described in Ref. 15 [15] was used to image the CBF axial velocity in penetrating vessels. A-line was repeated 25 times at each depth location to form 1 M-scan (z axis) at A-scan rate of 45 kHz. Each B-frame consisted of 300 M-scans, and a total of 300 B-frames (x axis) was acquired in the C-scan direction (y axis) with a scan rate of 6 fps. Thus, the final 3D volumetric data set took ~50 seconds to acquire and formed a cube of approximately 2 mm (x axis) x 2 mm (y axis) x 2.22mm (z axis).

4.3 Data analysis

To analyze multiple morphological and flow parameters in cerebral vessel networks, the methods described below were used. All the data processing was performed in customized MATLAB (MathWorks) programs and was visualized in the 3D software AMIRA (Visual Imaging).

4.3.1 Vein and artery diameter measurement

The vessel diameter was measured from OMAG angiograms obtained from enface projection images of 3D OMAG data within ~50 μm below the cortical surface. The angiograms were converted into black-and-white binary masks to accurately detect the vessel edges. To increase the comparison accuracy among different experimental regimes, vein and artery branches were classified according to branching order, in which segment 1 (Seg 1) was the most proximal and segment 3 (Seg 3) was the most distal. The diameters were calculated using MATLAB interactive distance tool that displayed the distance between line endpoints and compared among awake, ketamine-xylazine and isoflurane states. Finally, the diameter change index, ΔD, defined as

$$\Delta D = \frac{D_{anest} - D_{aw}}{D_{aw}},$$

where D_{anest} is the vessel diameter value at anesthetized state (isoflurane or ketamine-xylazine) and D_{aw} is the vessel diameter value at awake state, was compared for every vein and artery segment among three different regimes.

4.3.2 Capillary density and flux quantification

To quantify the capillary density, we used the vessel area density (VAD) method which was previously validated in OCT retina imaging and can be found in Ref. 47 [47]. First, enface projection images were reconstructed from 3D OMAG data set within ~250-μm-thick slab ~50 μm below the cortical surface (to exclude the meningeal vessels). Second, large vein and arterial vessels were excluded, so that only capillary network remained for the analysis. Next, with the application of global thresholding, Hessian filter and adaptive thresholding, the images were then converted into binary vessel area maps. The presence of functioning capillaries was indicated by a white pixel (value=1), while the absence was presented as a black pixel (value=0). The detected capillary vessels generated the capillary density map. Finally, the capillary VAD was calculated as a ratio of the region occupied by vessels (white pixels) to a given image region (2.5 mm×2.5 mm).

Capillary flux index was calculated based on flow signal intensity varying in the full dynamic range of 0-255. Then the signal was divided by 255, and thus normalized to the range from 0 to 1. Mean capillary flux index was obtained by averaging the normalized blood flow signal over the given area (2.5 mm×2.5 mm).[48] Both capillary VAD and mean capillary flux were compared among isoflurane, ketamine-xylazine and awake conditions.

4.3.3 CBF analysis

To assess CBF in penetrating vessels, we used the acquired DOMAG data. First, the axial RBC velocity, V_{axial}, An axial velocity range of -6mm/s to 6 mm/s was achieved by increasing time interval to a 3 A-line interval. To extract Doppler flow signal, a phase variance mask was used to eliminate the noisy background. Bidirectional axial velocity maps were constructed based on this signal. Next, an x-y orthogonal slice (2 mm×2 mm) ~50 μm below the cortical surface was selected from the 3D DOMAG data set and divided into 4 regions to quantify flow cross-sections at each region. Finally, the regional CBF was calculated by multiplying velocity and flow area measured within each region. The values were than normalized to a unit region (1 mm^2) and compared between awake and isoflurane groups.

4.3.4 Statistical analysis

The differences in vascular parameters between awake, ketamine-xylazine and isoflurane conditions were tested with One-way ANOVA followed by Tukey's honestly significant difference test for multiple comparisons. The differences in flow parameters between awake and isoflurane conditions were tested with Student's t test. $p<0.05$ was considered as statistically significant.

4.4 Results

4.4.1 Vessel dilation

To study the effect of anesthetics on vessel dilation, we measured the vessel diameter from OMAG angiograms at isoflurane, ketamine-xylazine and awake states. To make the comparison more accurate, the vein and artery branches were categorized according to branching order: segment 1 (Seg 1) as the most proximal, segment 2 (Seg 2) in the middle, and segment 3 (Seg 3) as the most

distal (Fig. 10A). Cross-sectional images of cortex structure and blood flow obtained with OCT are shown in Fig. 10B and Fig. 10C, respectively. OMAG angiograms were obtained from ~50 μm-thick slab indicated in Fig. 10C between yellow and blue lines. Angiograms in Fig. 10D-F correspond to isoflurane, ketamine-xylazine and awake states, accordingly. The vein and artery diameter values for Seg 1 (red), 2 (green) and 3 (purple) were measured from binary masks in Fig. 10G-I. ΔD was compared for every vein and artery segment among three different regimes (Fig.10K-L). Overall, there was an increasing trend from awake to isoflurane states. ΔD for vein Seg 3 at ketamine-xylazine was higher by 11% (p-value<0.0498) than at awake regime. ΔD for vein Seg 2 at isoflurane was higher by 6% (p-value<0.0430) than at ketamine-xylazine, and 22% higher (p-value<0.0198) than at awake state. ΔD for artery Seg 1 at isoflurane was higher by 12% (p-value<0.0352) than at ketamine-xylazine, and 29% higher (p-value<0.0104) than at awake state. These results showed that the vein and artery diameter increased at anesthetized states comparing to awake states, meaning that isoflurane and ketamine-xylazine caused significant vessel dilation.

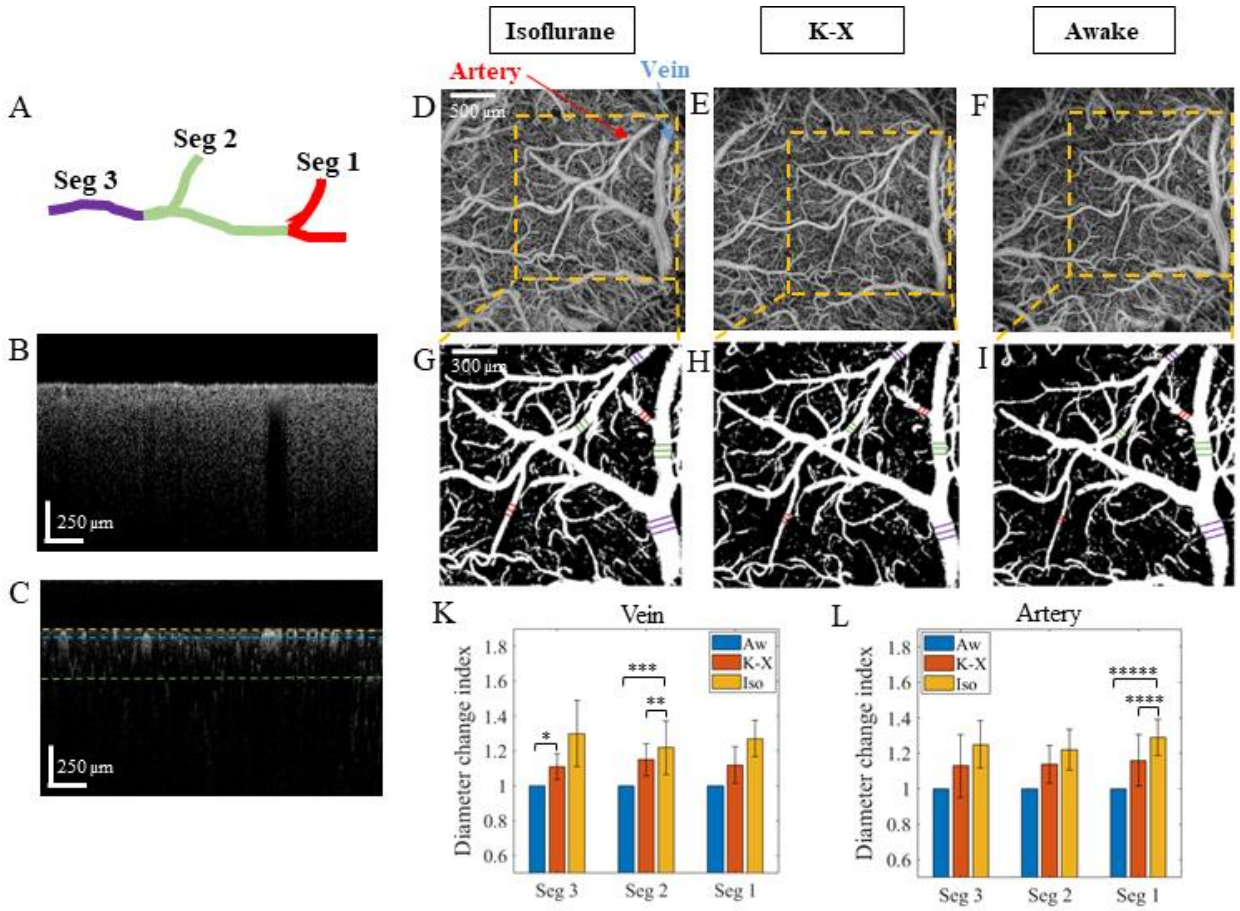

Figure 10. Comparison of artery and vein segment diameter. A. Classification of vessel branches with the most proximal branch assigned as segment 1 (Seg 1) and the most distal one as segment 3 (Seg 3). B. B-scan structural cross-section OCT image. C. B-scan flow cross-section OCT image. The yellow line indicates the cortical surface, while the blue and green lines are located at the depths of 50 and 300 μm from the cortical surface, respectively. D-F. OMAG angiograms corresponding to isoflurane, ketamine-xylazine, and awake states, respectively, obtained from enface mean intensity projection of 3-D OMAG datasets within a slab between yellow and blue dotted lines shown in C. Artery and vein are indicated in D with red and blue arrows, respectively. G-I. Vessel masks corresponding to D-F angiograms, respectively, with diameter length indicated in violet (Seg 3), green (Seg 2), and red (Seg 1). K-L. Comparison of diameter change index of vein and artery, respectively, for Seg 3, Seg 2 and Seg 1 among three different states. Aw – awake, K-X – Ketamine-Xylazine, Iso – isoflurane. *p-value<0.0498, **p-value<0.0430, ***p-value<0.0198, ****p-value<0. 0352, *****p-value<0.0104. The values are mean ± std. (standard deviation of group mean, N=6 animals per group).

4.4.2 Capillary density and flux

To compare the capillary density and flux parameters among three different states, OMAG angiograms (Fig. 11A-C) were processed to exclude big arteries and veins (Fig. 11D-F). The remaining capillary vessels generated the capillary density maps (Fig. 11G-I) and capillary flux maps (Fig. 11K-M) at isoflurane, ketamine-xylazine and awake conditions. Fig. 11N demonstrates

the flux index distributions at three different states fitted to Kernel distribution n. As it can be seen from this figure, flux index distribution at isoflurane had the largest population of flux index over the mean, while awake state had the smallest one. The comparisons of mean capillary density and mean flux index over the given region among three conditions are presented in Fig. 11O-P, respectively. The results showed that mean capillary density at awake state was lower by 23% than at ketamine-xylazine (p-value<0.0368) and by 25% than at isoflurane (p-value<0.0065). The mean flux index at awake state was lower by 5% than at ketamine-xylazine (p-value<0.0369) and by 15% than at isoflurane (p-value<0.0131). Overall, both capillary density and mean flux index increased from awake to anesthetized conditions.

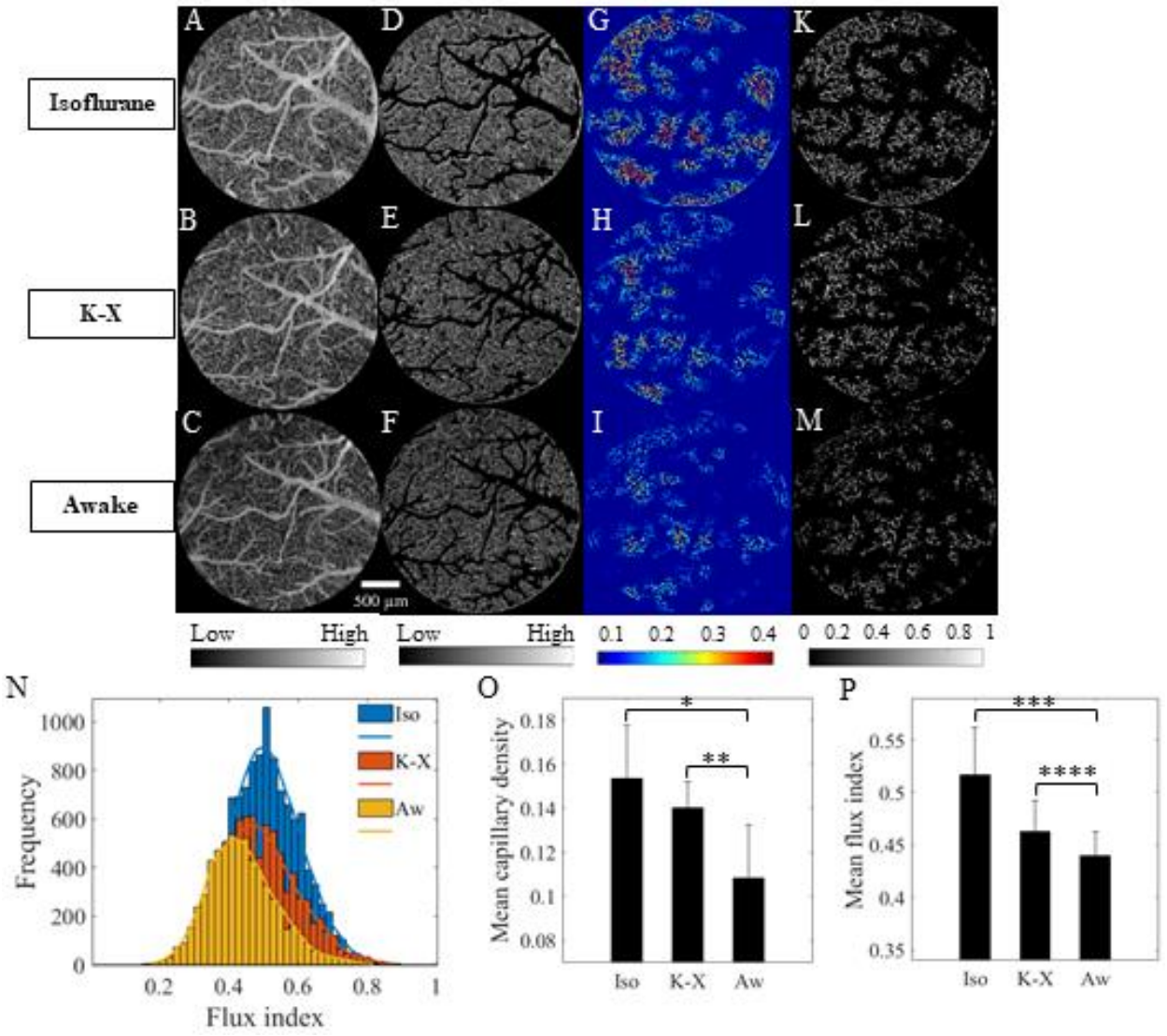

Figure 11. Comparison of cerebral capillary density and flux. A-C. OMAG angiograms corresponding to isoflurane, ketamine-xylazine, and awake states, respectively, obtained from *enface* maximum intensity projection of 3-D OMAG datasets within a 50-300 μm slab. D-F. OMAG angiograms with arteries and veins excluded corresponding to isoflurane, ketamine-xylazine, and awake states, respectively. G-I. Color index-coded capillary density maps of three states. K-M. Capillary flux maps of three states. N. Capillary flux histogram distributions of three states fitted to Kernel distribution. O. Comparison of mean capillary density among three states. *p-value<0.0065, **p-value<0.0368. P. Comparison of mean flux among three states. *p-value<0.0131, **p-value<0.0369. The values are mean ± std. (standard deviation of group mean, N=6 animals per group).

4.4.3 CBF measurements from penetrating vessels

To assess the CBF difference between awake and anesthetized regimes, we quantified the axial velocity of RBCs, flow cross-section area, and total blood flow from DOMAG angiograms.

Figures 12A-B reveal the bidirectional enface DOMAG axial velocity maps at isoflurane and awake regimes. Diving arterioles and rising venules are displayed in green and red colors, respectively, and the axial flow velocity information is coded with a color bar in a range of ±6 mm/s. Orthogonal slices extracted from 3D slab in Fig. 12C were produced (Fig. 12D-E) to compare the mean axial velocity (Fig. 12F), flow cross-section area (Fig. 12G) and total blood flow (Fig. 12H) over four regions between awake and isoflurane regimes. While mean velocity value increased only by 3% from awake to isoflurane state, the flow cross-section area value increased by 57% ($p<0.04$) and total blood flow increased by 55% ($p<0.04$). In addition, as it can be seen from Fig. 12A-B and Fig. 12D-E, the penetration vessel density increased from awake to isoflurane state, which supports the results related to capillary VAD in Fig. 11G-I.

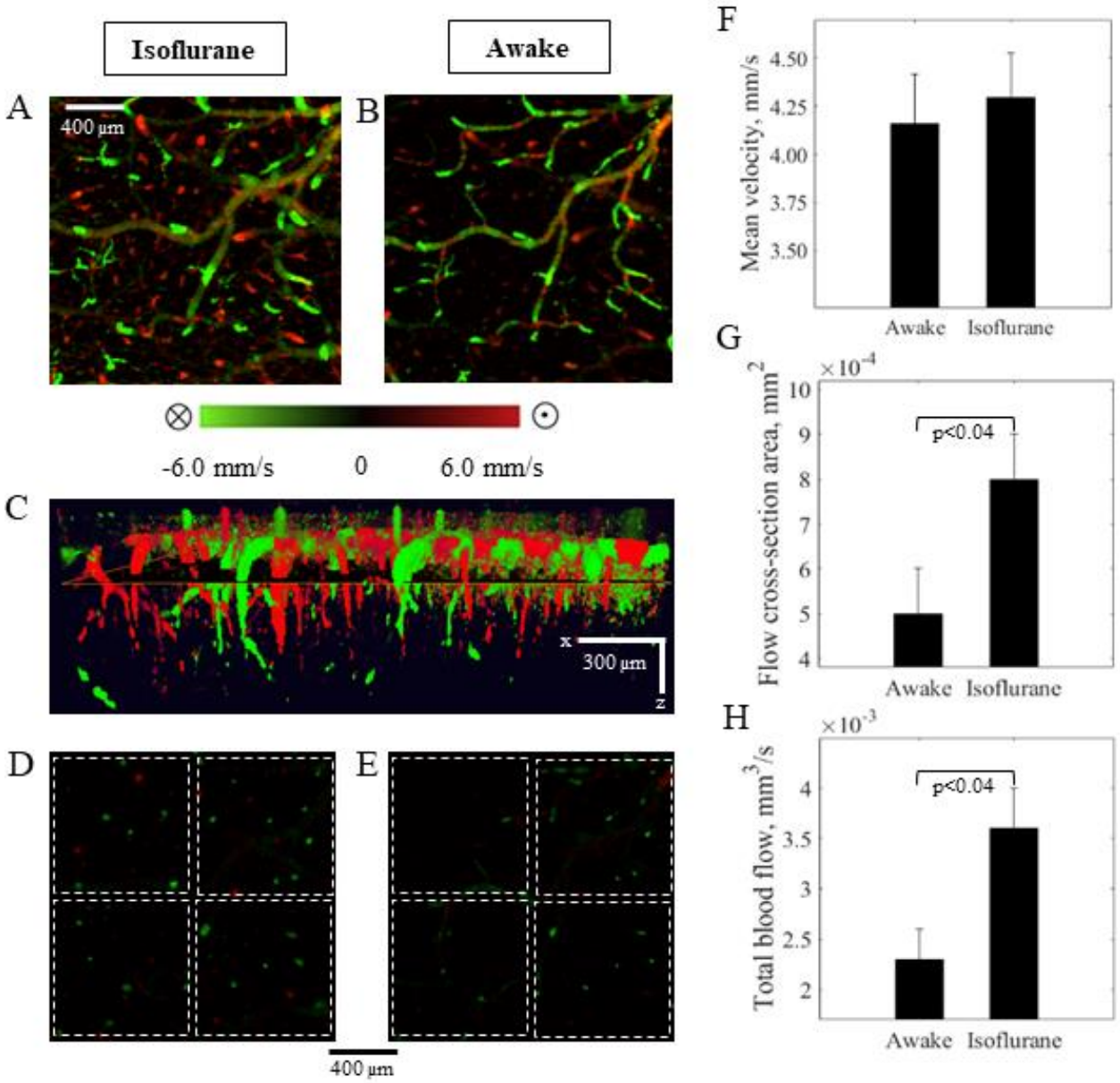

Figure 12. Comparison of CBF parameters. A-B. Bidirectional axial CBF velocity maps of mouse cortex at isoflurane and awake regimes, correspondingly, generated by *enface* maximum intensity projection of 3D DOMAG datasets within a slab demonstrated in C. Color bar represents the axial velocity of RBCs moving down (negative, green) and up (positive, red) in a range of ±6.0 mm/s. The yellow color is a mix of green and red signals from the projection effect. C. 3D visualization of 300-µm thick slab generated from 3D DOMAG dataset with descending and ascending vessels. D-E. Orthogonal slices from C at an x-y plane ~50 mm below the cortical surface at isoflurane and awake regimes, respectively. Green and red dots represent the cross sections of vessel flows. F-H. Comparison of mean axial velocity, flow cross-section area, and total blood flow, accordingly, between awake and isoflurane regimes.

4.5 Discussion

Imaging CBF in *in vivo* animal models plays a key role in neurovascular studies. Although the use of anesthetized animals are frequently preferred for optical imaging experiments due to the ability to restrain the animals and release them from stress, there is evidence that different anesthetic agents have a profound effect on the animal physiology.[39] As a result, the CBF regulation is considerably influenced by anesthesia which might affect the experimental outcome. [40] There has been little quantitative analysis of the difference in cerebral blood vessel morphology and flow between awake and anesthetized regimes, which served us as a motivation to conduct this study with OCT.

In contrast to other optical imaging modalities, OCT allows wide-field microscale visualization in combination with fast-speed 3D data acquisition. With its recent OCTA advancements, it is possible to image the cerebral vessel networks down to capillary level and evaluate CBF deep into cortical layers. [9] In this study, we used OMAG and DOMAG imaging methods to quantitatively characterize the differences in cerebral vasculature and blood flow among three experimental regimes – awake, ketamine-xylazine anesthesia and isoflurane anesthesia.

Isoflurane and ketamine-xylazine are the most used anesthetics in biomedical research. Isoflurane is a volatile agent frequently utilized in cardiovascular research experiments since it does not depress the cardiac function as much as injectable anesthetic agents. Nevertheless, volatile anesthetics are known to impair cerebral autoregulation [49], and therefore, not preferred in neurovascular coupling studies. Isoflurane was proven to induce the relaxation of cerebral blood vessels (arteries and parenchymal arterioles) via its effect on ATP-sensitive potassium channels

and decrease calcium current in smooth muscle cells. [40, 50-51] Injectable anesthetics based on the combination with ketamine are more likely to preserve autoregulatory responses. However, they were also shown to have vasodilatory effect, which was suggestively explained by partial interference with transmembrane influx of Ca^{+} and the activation of cholinergic cerebral vasodilator system. [52-53] Our OMAG results (Fig.10K-L) demonstrated that the largest vasodilation of both veins and arteries was caused by isoflurane. Ketamine-xylazine also induced the increase of vessel dimensions, yet to a lesser degree.

The cerebral capillary density was quantified at the same cortical layer across three different regimes. According to our results, mean capillary density increased from awake to ketamine-xylazine and from ketamine-xylazine to isoflurane condition (Fig. 11O). This indicates a growth in capillary vessel area from awake to anesthetized state, meaning that capillary vessels dilated as well.

The latter result supports another important finding in our study. The measured mean flux index in capillaries at awake regime was lower than at ketamine-xylazine and isoflurane regimes (Fig. 11N, P). The mean flux index is based on blood flow signal intensity which is proportional to the number of RBCs passing through the vessels. [48] Therefore, we might assume that capillary vasodilation caused the growth of RBC amount in capillaries during anesthesia.

Cerebral vasodilation results in decreased arterial pressure, which subsequently elevates CBF and peripheral blood perfusion. [54] In the current study, the CBF difference in penetrating vessels between awake and anesthetized conditions was assessed using DOMAG technique. While mean axial velocity of RBCs did not change significantly from awake to isoflurane state (Fig. 12F), the flow cross-section area increased by 57% (Fig. 12G) presumably caused by vessel dilation observed in Fig. 3. Since total blood flow in penetrating vessels was calculated as a product of

RBC axial velocity and flow cross-section area, total blood flow also escalated by 55% (Fig. 12H). Number of studies report the increase of baseline CBF due to anesthesia effect. For example, Drummond et al. [55] observed an elevation of CBF in rabbits by ~58% after the administration of 0.75 minimum alveolar anesthetic concentration (MAC) of isoflurane and by ~72% after halothane. Functional MRI study showed that CBF was obviously higher under isoflurane-anesthetized condition compared with the awake state. [56] The review on ketamine effect on CBF [57] provided a summary of seventeen animal studies demonstrated either a regional or global increase in CBF during ketamine administration.

Thus, the use of anesthetics such as isoflurane and ketamine-xylazine can cause abnormal cerebrovascular response and alter the baseline CBF. However, despite the rapid development of head-restraining techniques, the transition to fully awake imaging can still be challenging. Awake imaging induces significant restraint-related stress and discomfort to animals, which can contaminate the obtained signals. [58] Anesthesia-effect studies report that the contribution of anesthetic agents is dose dependent. For example, low isoflurane concentration (1.3%-1.5%) maintains CBF values close to those of the awake condition. [40] Hence, the decision on an experimental regime should arise from an experiment type and the purpose of study. In addition, it is suggested to perform experiments under different experimental conditions and compare the obtained results to produce reliable results. [59]

4.6 Conclusion

Most *in vivo* optical imaging studies are performed in anesthetized animals. Anesthesia was proven to cause abnormal vascular response and flow dynamics change in brain cortex. Therefore, it is important to quantitatively characterize the anesthesia effect in animal models. In this study, we

used OCTA techniques to measure and compare the baseline morphological and flow parameters in mouse cerebral vascular networks between awake and anesthetized conditions. Our results showed that isoflurane and ketamine-xylazine caused vasodilation both in large and capillary vessels. The increase of vessel dimensions resulted in increase of CBF. In conclusion, we believe that our quantitative comparison study will help researchers to choose an appropriate experimental protocol for neurovascular studies.

Chapter 5. SUMMARY

To sum up, studying cerebral hemodynamics both at basal and neural activation conditions is important for understanding the neurovascular relationship in brain. Number of *in vivo* imaging modalities serve this purpose. However, all of them come with certain limitations such as low spatial and temporal resolution, requirement of physical contact or contrast agent injection, no access to deep-layer structures and insufficient FOV. Enabling high-resolution 3D visualization and quantification of microvascular networks, OCT fills the given gap. In this thesis, the application of OCTA methods in studying CBF in mouse model was discussed. Using OMAG, the temporal profile of hemodynamic change in response to neural activation and the variation of depth-resolved blood flow changes in mouse cerebral cortex was investigated. OMAG and DOMAG techniques were also applied to compare cerebral vessel morphology and blood flow between awake and anesthetized regimes in mouse model. Overall, optical microangiography is an effective tool for studying depth resolved blood flow in cerebral cortex in animals. It has a great potential to provide the insights of hemodynamic events associated with the NVC.

Bibliography

[1] Attwell, D., Buchan, A.M., Charpak, S., Lauritzen, M., Macvicar, B.A. & Newman, E. A. (2010). Glial and neuronal control of brain blood flow. Nature, 468(7321), 232–243.

[2] Ogawa, S., Menon, R. S., Tank, D. W., Kim, S. G., Merkle, H., Ellermann, J. M., & Ugurbil, K. (1993). Functional brain mapping by blood oxygenation level-dependent contrast magnetic resonance imaging. A comparison of signal characteristics with a biophysical model. Biophysical journal, 64(3), 803-812.

[3] Heiss, W. D., Graf, R., Wienhard, K., Löttgen, J., Saito, R., Fujita, T., ... & Wagner, R. (1994). Dynamic penumbra demonstrated by sequential multitracer PET after middle cerebral artery occlusion in cats. Journal of Cerebral Blood Flow & Metabolism, 14(6), 892-902.

[4] Dirnagl, U., Kaplan, B., Jacewicz, M., & Pulsinelli, W. (1989). Continuous measurement of cerebral cortical blood flow by laser—Doppler flowmetry in a rat stroke model. Journal of Cerebral Blood Flow & Metabolism, 9(5), 589-596.

[5] Zhang, H. F., Maslov, K., Stoica, G., & Wang, L. V. (2006). Functional photoacoustic microscopy for high-resolution and noninvasive in vivo imaging. Nature biotechnology, 24(7), 848-851.

[6] Lu, H. D., Chen, G., Cai, J., & Roe, A. W. (2017). Intrinsic signal optical imaging of visual brain activity: tracking of fast cortical dynamics. NeuroImage, 148, 160-168.

[7] Dunn, A. K., Bolay, H., Moskowitz, M. A., & Boas, D. A. (2001). Dynamic imaging of cerebral blood flow using laser speckle. Journal of Cerebral Blood Flow & Metabolism, 21(3), 195-201.

[8] Kleinfeld, D., Mitra, P. P., Helmchen, F., & Denk, W. (1998). Fluctuations and stimulus-induced changes in blood flow observed in individual capillaries in layers 2 through 4 of rat neocortex. Proceedings of the National Academy of Sciences, 95(26), 15741-15746.

[9] Shih, A. Y., Driscoll, J. D., Drew, P. J., Nishimura, N., Schaffer, C. B., & Kleinfeld, D. (2012). Two-photon microscopy as a tool to study blood flow and neurovascular coupling in the rodent brain. Journal of Cerebral Blood Flow & Metabolism, 32(7), 1277-1309.

[10] Gao, Y. R., Greene, S. E., & Drew, P. J. (2015). Mechanical restriction of intracortical vessel dilation by brain tissue sculpts the hemodynamic response. Neuroimage, 115, 162-176.

[11] Pérez-Alvarez, A., Araque, A., & Martín, E. D. (2013). Confocal microscopy for astrocyte in vivo imaging: recycle and reuse in microscopy. Frontiers in cellular neuroscience, 7, 51.

[12] Tsai, P. S., Mateo, C., Field, J. J., Schaffer, C. B., Anderson, M. E., & Kleinfeld, D. (2015). Ultra-large field-of-view two-photon microscopy. Optics express, 23(11), 13833-13847.

[13] Wang, R. K., Jacques, S. L., Ma, Z., Hurst, S., Hanson, S. R., & Gruber, A. (2007). Three dimensional optical angiography. Optics express, 15(7), 4083-4097.

[14] Wang, R. K. (2009). Optical microangiography: a label-free 3-D imaging technology to visualize and quantify blood circulations within tissue beds in vivo. IEEE Journal of Selected Topics in Quantum Electronics, 16(3), 545-554.

[15] Shi, L., Qin, J., Reif, R., & Wang, R. K. (2013). Wide velocity range Doppler optical microangiography using optimized step-scanning protocol with phase variance mask. Journal of biomedical optics, 18(10), 106015.

[16] Frostig, R. D., Masino, S. A., Kwon, M. C., & Chen, C. H. (1995). Using light to probe the brain: Intrinsic signal optical imaging. International Journal of Imaging Systems and Technology, 6(2-3), 216-224.
[17] Bouchard, M. B., Chen, B. R., Burgess, S. A., & Hillman, E. M. (2009). Ultra-fast multispectral optical imaging of cortical oxygenation, blood flow, and intracellular calcium dynamics. Optics express, 17(18), 15670-15678.
[18] Fujimoto, J. G., Pitris, C., Boppart, S. A., & Brezinski, M. E. (2000). Optical coherence tomography: an emerging technology for biomedical imaging and optical biopsy. Neoplasia (New York, NY), 2(1-2), 9.
[19] Leitgeb, R., Hitzenberger, C. K., & Fercher, A. F. (2003). Performance of fourier domain vs. time domain optical coherence tomography. Optics express, 11(8), 889-894.
[20] Zhu, J., Merkle, C. W., Bernucci, M. T., Chong, S. P., & Srinivasan, V. J. (2017). Can OCT angiography be made a quantitative blood measurement tool?. Applied Sciences, 7(7), 687.
[21] Yousefi, S., Zhi, Z., & Wang, R. K. (2011). Eigendecomposition-based clutter filtering technique for optical microangiography. IEEE transactions on biomedical engineering, 58(8), 2316-2323.
[22] Wang, R. K., & An, L. (2009). Doppler optical micro-angiography for volumetric imaging of vascular perfusion in vivo. Optics express, 17(11), 8926-8940.
[23] Srinivasan, V. J., Sakadžić, S., Gorczynska, I., Ruvinskaya, S., Wu, W., Fujimoto, J. G., & Boas, D. A. (2010). Quantitative cerebral blood flow with optical coherence tomography. Optics express, 18(3), 2477-2494.
[24] De Kock, C. P. J., Bruno, R. M., Spors, H., & Sakmann, B. (2007). Layer-and cell-type-specific suprathreshold stimulus representation in rat primary somatosensory cortex. The Journal of physiology, 581(1), 139-154.
[25] Goense, J., Merkle, H., & Logothetis, N. K. (2012). High-resolution fMRI reveals laminar differences in neurovascular coupling between positive and negative BOLD responses. Neuron, 76(3), 629-639.
[26] Tian, P., Teng, I. C., May, L. D., Kurz, R., Lu, K., Scadeng, M., ... & Marota, J. J. (2010). Cortical depth-specific microvascular dilation underlies laminar differences in blood oxygenation level-dependent functional MRI signal. Proceedings of the National Academy of Sciences, 107(34), 15246-15251.
[27] Gutiérrez-Jiménez, E., Cai, C., Mikkelsen, I. K., Rasmussen, P. M., Angleys, H., Merrild, M., ... & Sakadzic, S. (2016). Effect of electrical forepaw stimulation on capillary transit-time heterogeneity (CTH). Journal of Cerebral Blood Flow & Metabolism, 36(12), 2072-2086.
[28] Merkle, C. W., & Srinivasan, V. J. (2016). Laminar microvascular transit time distribution in the mouse somatosensory cortex revealed by Dynamic Contrast Optical Coherence Tomography. Neuroimage, 125, 350-362.
[29] Baran, U., Li, Y., & Wang, R. K. (2015). Vasodynamics of pial and penetrating arterioles in relation to arteriolo-arteriolar anastomosis after focal stroke. Neurophotonics, 2(2), 025006.
[30] Li, Y., Wei, W., & Wang, R. K. (2018). Capillary flow homogenization during functional activation revealed by optical coherence tomography angiography based capillary velocimetry. Scientific reports, 8(1), 1-9.
[31] Li, Y., Baran, U., & Wang, R. K. (2014). Application of thinned-skull cranial window to mouse cerebral blood flow imaging using optical microangiography. PLoS One, 9(11).

[32] Takuwa, H., Autio, J., Nakayama, H., Matsuura, T., Obata, T., Okada, E., ... & Kanno, I. (2011). Reproducibility and variance of a stimulation-induced hemodynamic response in barrel cortex of awake behaving mice. Brain research, 1369, 103-111.
[33] "Allen Brain Atlas: Mouse Brain," Allen Institute for Brain Science. Accessed December 9, 2019. https://mouse.brain-map.org/static/atlas.
[34] Choi, W. J., Qin, W., Chen, C. L., Wang, J., Zhang, Q., Yang, X., ... & Wang, R. K. (2016). Characterizing relationship between optical microangiography signals and capillary flow using microfluidic channels. Biomedical optics express, 7(7), 2709-2728.
[35] Yang, J., Su, J., Wang, J., Men, S., Jia, Y., Huang, D., & Liu, G. (2017). Hematocrit dependence of flow signal in optical coherence tomography angiography. Biomedical optics express, 8(2), 776-789.
[36] Harrison, R. V., Harel, N., Panesar, J., & Mount, R. J. (2002). Blood capillary distribution correlates with hemodynamic-based functional imaging in cerebral cortex. Cerebral Cortex, 12(3), 225-233.
[37] Hillman, E. M., Devor, A., Bouchard, M. B., Dunn, A. K., Krauss, G. W., Skoch, J., ... & Boas, D. A. (2007). Depth-resolved optical imaging and microscopy of vascular compartment dynamics during somatosensory stimulation. Neuroimage, 35(1), 89-104.
[38] Srinivasan, V. J., & Radhakrishnan, H. (2014). Optical Coherence Tomography angiography reveals laminar microvascular hemodynamics in the rat somatosensory cortex during activation. NeuroImage, 102, 393-406.
[39] Blinder, P., Tsai, P. S., Kaufhold, J. P., Knutsen, P. M., Suhl, H., & Kleinfeld, D. (2013). The cortical angiome: an interconnected vascular network with noncolumnar patterns of blood flow. Nature neuroscience, 16(7), 889.
[40] Slupe, A. M., & Kirsch, J. R. (2018). Effects of anesthesia on cerebral blood flow, metabolism, and neuroprotection. Journal of Cerebral Blood Flow & Metabolism, 38(12), 2192-2208.
[41] Masamoto, K., & Kanno, I. (2012). Anesthesia and the quantitative evaluation of neurovascular coupling. Journal of Cerebral Blood Flow & Metabolism, 32(7), 1233-1247.
[42] Pisauro, M. A., Dhruv, N. T., Carandini, M., & Benucci, A. (2013). Fast hemodynamic responses in the visual cortex of the awake mouse. Journal of Neuroscience, 33(46), 18343-18351.
[43] Sharp, P. S., Shaw, K., Boorman, L., Harris, S., Kennerley, A. J., Azzouz, M., & Berwick, J. (2015). Comparison of stimulus-evoked cerebral hemodynamics in the awake mouse and under a novel anesthetic regime. Scientific reports, 5, 12621.
[44] Gao, Y. R., Ma, Y., Zhang, Q., Winder, A. T., Liang, Z., Antinori, L., ... & Zhang, N. (2017). Time to wake up: Studying neurovascular coupling and brain-wide circuit function in the un-anesthetized animal. Neuroimage, 153, 382-398.
[45] Martin, C., Martindale, J., Berwick, J., & Mayhew, J. (2006). Investigating neural–hemodynamic coupling and the hemodynamic response function in the awake rat. Neuroimage, 32(1), 33-48.
[46] Santisakultarm, T. P., Kersbergen, C. J., Bandy, D. K., Ide, D. C., Choi, S. H., & Silva, A. C. (2016). Two-photon imaging of cerebral hemodynamics and neural activity in awake and anesthetized marmosets. Journal of neuroscience methods, 271, 55-64.
[47] Cao, R., Li, J., Ning, B., Sun, N., Wang, T., Zuo, Z., & Hu, S. (2017). Functional and oxygen-metabolic photoacoustic microscopy of the awake mouse brain. Neuroimage, 150, 77-87.

[48] Chu, Z., Lin, J., Gao, C., Xin, C., Zhang, Q., Chen, C. L., ... & Wang, R. K. (2016). Quantitative assessment of the retinal microvasculature using optical coherence tomography angiography. Journal of biomedical optics, 21(6), 066008.
[49] Chen, C. L., Bojikian, K. D., Gupta, D., Wen, J. C., Zhang, Q., Xin, C., ... & Wang, R. K. (2016). Optic nerve head perfusion in normal eyes and eyes with glaucoma using optical coherence tomography-based microangiography. Quantitative imaging in medicine and surgery, 6(2), 125.
[50] Hoffmann, U., Sheng, H., Ayata, C., & Warner, D. S. (2016). Anesthesia in experimental stroke research. Translational stroke research, 7(5), 358-367.
[51] Iida, H., Ohata, H., Iida, M., Watanabe, Y., & Dohi, S. (1998). Isoflurane and sevoflurane induce vasodilation of cerebral vessels via ATP-sensitive K+ channel activation. Anesthesiology: The Journal of the American Society of Anesthesiologists, 89(4), 954-960.
[52] Flynn, N. M., Bulijubasic, N., Bosnjak, Z. J., & Kampine, J. P. (1992). Isoflurane Produces Endothelium-independent Relaxation inCanine Middle Cerebral Arteries. Anesthesiology: The Journal of the American Society of Anesthesiologists, 76(3), 461-467.
[53] Oren, R. E., Rasool, N. A., & Rubinstein, E. H. (1987). Effect of ketamine on cerebral cortical blood flow and metabolism in rabbits. Stroke, 18(2), 441-444.
[54] Akata, T., Izumi, K., & Nakashima, M. (2001). Mechanisms of direct inhibitory action of ketamine on vascular smooth muscle in mesenteric resistance arteries. ANESTHESIOLOGY-PHILADELPHIA THEN HAGERSTOWN-, 95(2), 452-462.
[55] Tremoleda, J. L., Kerton, A., & Gsell, W. (2012). Anaesthesia and physiological monitoring during in vivo imaging of laboratory rodents: considerations on experimental outcomes and animal welfare. EJNMMI research, 2(1), 44.
[56] Drummond, J. C., Todd, M. M., Scheller, M. S., & Shapiro, H. M. (1986). A comparison of the direct cerebral vasodilating potencies of halothane and isoflurane in the New Zealand white rabbit. Anesthesiology: The Journal of the American Society of Anesthesiologists, 65(5), 462-467.
[57] Sicard, K., Shen, Q., Brevard, M. E., Sullivan, R., Ferris, C. F., King, J. A., & Duong, T. Q. (2003). Regional cerebral blood flow and BOLD responses in conscious and anesthetized rats under basal and hypercapnic conditions: implications for functional MRI studies. Journal of Cerebral Blood Flow & Metabolism, 23(4), 472-481.
[58] Zeiler, F. A., Sader, N., Gillman, L. M., Teitelbaum, J., West, M., & Kazina, C. J. (2016). The cerebrovascular response to ketamine: a systematic review of the animal and human literature. Journal of neurosurgical anesthesiology, 28(2), 123-140.
[59] Lahti, K. M., Ferris, C. F., Li, F., Sotak, C. H., & King, J. A. (1999). Comparison of evoked cortical activity in conscious and propofol-anesthetized rats using functional MRI. Magnetic Resonance in Medicine: An Official Journal of the International Society for Magnetic Resonance in Medicine, 41(2), 412-416.